



# Mercury sources, transport, and transformation in rainfall-runoff processes: Mercury isotope approach

Ruolan Li<sup>a,b</sup>, Junyao Yan<sup>a,b</sup>, Chuan Wang<sup>a,b</sup>, Shaochen Yang<sup>a</sup>, Lin Zhang<sup>a,c</sup>, Tao Peng<sup>a,c</sup>, Wei Zhu<sup>d</sup>, Ping Li<sup>a,\*</sup>, Leiming Zhang<sup>e</sup>, Xinbin Feng<sup>a,b</sup>

<sup>a</sup> State Key Laboratory of Environmental Geochemistry, Institute of Geochemistry, Chinese Academy of Sciences, Guiyang 550081, China

<sup>b</sup> University of Chinese Academy of Sciences, Beijing 100049, China

<sup>c</sup> Puding Karst Ecosystem Research Station, Chinese Academy of Sciences, Puding 562100, China

<sup>d</sup> Department of Forest Ecology and Management, Swedish University of Agricultural Sciences, Umeå SE-90183, Sweden

<sup>e</sup> Air Quality Research Division, Science and Technology Branch, Environment and Climate Change Canada, Toronto M3H5T4, Canada

## ARTICLE INFO

### Keywords:

Watershed  
Mercury isotope  
Source apportionment  
Water mercury dynamics

## ABSTRACT

Mercury (Hg) in runoff water poses significant ecological risks to aquatic ecosystems that can affect organisms. However, accurately identifying the sources and transformation processes of Hg in runoff water is challenging due to complex natural conditions. This study provides a comprehensive investigation of Hg dynamics in water from rainfall to runoff. The Hg isotope fractionation in water was characterized, which allows accurate quantification of Hg sources, transport, and transformations in rainfall-runoff processes.  $\Delta^{200}\text{Hg}$  and corrected  $\Delta^{199}\text{Hg}$  values can serve as reliable tracers for identifying Hg sources in the runoff water and the variation of  $\delta^{202}\text{Hg}$  can be explained by Hg transformation processes. During runoff migration processes, Hg from rainfall is rapidly absorbed on the land surface, while terrestrial Hg entering the water by the dissolution process becomes the primary component of dissolved mercury (DHg). Besides the dissolution and adsorption, microbial Hg(II) reduction and demethylation of MeHg were dominant processes for DHg in the runoff water that flows through the rice paddies, while photochemical Hg(II) reduction was the dominant process for DHg in the runoff water with low water exchange rates. Particulate Hg (PHg) in runoff water is dominantly originated by the terrestrial material and derived from the dissolution and adsorption process. Tracking sources and transformations of Hg in runoff water during the rainfall-runoff process provides a basis for studying Hg pollution in larger water bodies under complex environmental factors.

## 1. Introduction

Mercury (Hg) in aquatic environments is a significant concern due to its bioaccumulation in organisms through the food chain (Beckers and Rinklebe, 2017; Gao et al., 2018; Liu et al., 2014). Terrestrial Hg inputs, atmospheric dry and wet (i.e., rainfall) deposition, and direct anthropogenic wastewater discharges are considered to be sources of Hg in aquatic ecosystems (Bishop et al., 2020; Obrist et al., 2018). In remote and regional background areas, terrestrial sources of Hg input through erosion during the rainfall-runoff process are the main sources of Hg in runoff water, contributing more than 80% (Tsui et al., 2020; Woerndle et al., 2018; Xia et al., 2022; Yuan et al., 2024). Rainfall-runoff process plays a significant role in importing terrestrial sources of Hg into aquatic systems.

When rain falls, a portion of it infiltrates into the soil, to replenish as groundwater, while the rest travels as surface runoff, particularly when the soil is saturated or impermeable. Several physiochemical and microbial transformation processes, including desorption and adsorption of Hg, Hg(II) reduction, Hg(II) methylation, and methylmercury (MeHg) demethylation may occur during rainfall-runoff process (Aleku et al., 2024; Luo et al., 2020; Zhang et al., 2020a). The Hg dynamics of runoff water is affected by various factors, including soil characteristics, land use, vegetation cover, topography, and the intensity and duration of rainfall (Gebka et al., 2019; Gebka et al., 2020; Qiao et al., 2023). In forests and peatlands, Hg fluxes measurements indicated that Hg from rainfall is largely retained in the canopy and rainforest floor (Sun et al., 2019; Wang et al., 2022; Yuan et al., 2024). However, it remains a gap in the systematic quantification and understanding of the Hg sources,

\* Corresponding author.

E-mail address: [liping@mail.gyig.ac.cn](mailto:liping@mail.gyig.ac.cn) (P. Li).

<https://doi.org/10.1016/j.watres.2024.122044>

Received 21 March 2024; Received in revised form 25 June 2024; Accepted 2 July 2024

Available online 4 July 2024

0043-1354/© 2024 Elsevier Ltd. All rights reserved, including those for text and data mining, AI training, and similar technologies.

transport, and transformation in runoff water during the whole rainfall-runoff process.

Stable Hg isotopes are powerful tools for tracing Hg sources and processes (Yin et al., 2010b). Mass-dependent fractionation (MDF, reported as  $\delta^{202}\text{Hg}$ ) and mass-independent fractionation (MIF, reported as  $\Delta^{199}\text{Hg}$  and  $\Delta^{201}\text{Hg}$  for odd-MIF, and  $\Delta^{200}\text{Hg}$  and  $\Delta^{204}\text{Hg}$  for even-MIF) occur in various Hg chemical and biological transformation processes (Blum et al., 2014). Hg isotope signals of runoff water resulted from combined impacts including the mixing of different sources and transformation processes.  $\Delta^{200}\text{Hg}$  is a favorable conservative parameter for distinguishing rainfall and terrestrial Hg sources (Cai and Chen, 2016; Yuan et al., 2024). When distinguishing specific terrestrial Hg sources, the main controlling factors (source mixing and transformation processes) of other signals, such as  $\Delta^{199}\text{Hg}$  and  $\delta^{202}\text{Hg}$  in runoff water, must be clarified before they can be used as quantitative parameters for identifying Hg sources. In natural water, photochemical Hg(II) reduction (Bergquist and Blum, 2007; Motta et al., 2020; Zheng and Hintelmann, 2009) and dark abiotic Hg(II) reduction (Schwab et al., 2023; Zheng and Hintelmann, 2010b) can result in significant odd-MIF and MDF. Microbial Hg(II) reduction (Kritee et al., 2007), dissolution (Brocza et al., 2019; Yin et al., 2013), adsorption, desorption (Wiederhold et al., 2010), methylation of Hg(II) (Rodríguez-González et al., 2009), and demethylation of MeHg (Kritee et al., 2009) only result in

significant MDF. Combining MDF with MIF allows the distinction of different processes.

This study aims to identify the dominant factors affecting the Hg isotopic composition of runoff water during the whole rainfall-runoff process, and trace and quantify the source, transport, and transformation of Hg in runoff water. We selected a watershed area in a karst basin with no industrial wastewater input, which enables us to trace the whole runoff process from generation to convergence (Chen et al., 2018). The characteristic spatial Hg concentrations and isotopic compositions of water at various locations along the runoff migration were observed. Our results provide the scientific basis for accurately understanding Hg contamination of runoff water in aquatic ecosystems.

## 2. Materials and methods

### 2.1. Study area

The Chenqi watershed ( $26^{\circ}15'44''\text{N}$ ,  $105^{\circ}46'22''\text{E}$ ), located in Puding County, Guizhou Province, southwest China, is part of the Wujiang River system in the Yangtze River Basin. This distinctive watershed, featuring conical hills and star-shaped valleys, is an excellent illustration of a karst plateau ecosystem, covering an area of only 1.2 km<sup>2</sup> (Cao et al., 2020; Chen et al., 2018; Zhang et al., 2011). The area has a subtropical humid

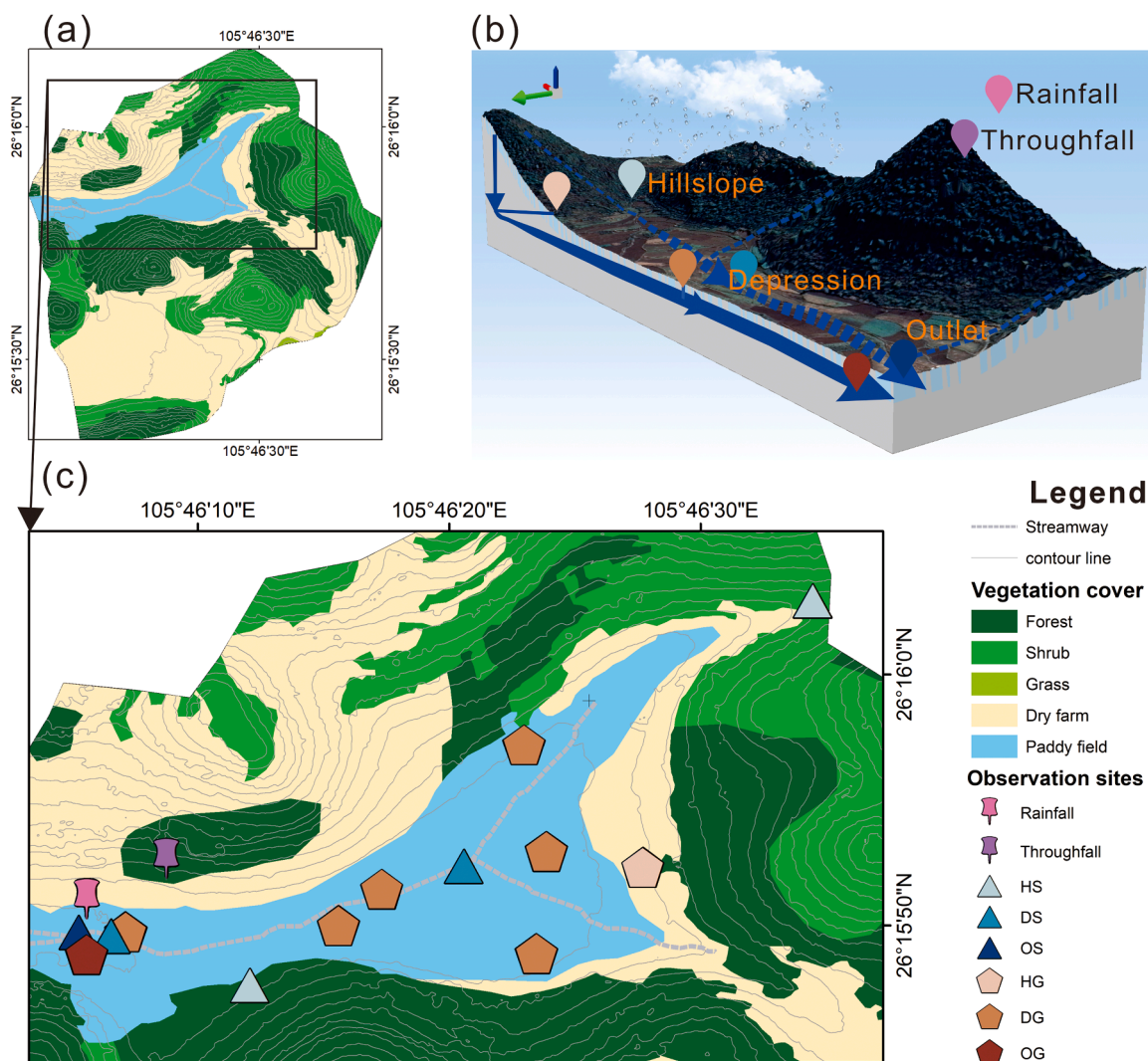


**Fig. 1.** Observation Sites of the Hydrological Runoff Process in Chenqi Watershed. (a) Overview of the watershed area. (b) The migration relationship between observed runoff sites in the rainfall-runoff process. (Cao et al., 2020; Chen et al., 2018; Cheng et al., 2020). (c) Distribution of actual sampling sites. Note that in the abbreviations for runoff sites, H, D, and O stand for hillslope, depression, and outlet; S, and G for surface water and groundwater respectively.

monsoon climate, with an average annual rainfall of 1315 mm and a temperature of 15.1 °C (Zhao et al., 2010). Over 80% of the annual rainfall occurs during the rainy season from May to October (Zhao et al., 2010). The geological composition of the basin is diverse, which includes dolomite, thick and thin-bedded limestone, marl, and Quaternary soils (Zhang et al., 2019). The predominant soil types are limestone soils (93%) and paddy soils (Gong et al., 2019). In high-elevation hillslopes (1340–1500 m), the topsoil layer is relatively thin (< 50 cm), with carbonate rocks exposed, and the dominant vegetation is deciduous broadleaf trees and various types of shrubs. In low-elevation depression areas (<1340 m), soil layers are thick (>1 m), and are primarily used for agricultural planting, such as corn and rice (Zhang et al., 2019; Zhao et al., 2015) (Fig. 1a).

A wealth of hydrological runoff process observation points is distributed in the Chenqi watershed, helping us to observe the entire process of Hg changes in water bodies from rainfall to runoff. The hillside and depression units serve as runoff generation and convergence areas of the watershed, respectively. In this study, the rainfall-runoff process in the watershed is simplified and categorized based on the characteristics of runoff generation and convergence, as illustrated in Fig. 1b. In the hillside unit, a portion of the rainfall that reaches the ground generates surface runoff (hillslope surface runoff, HS), while the remainder infiltrates the soil and rock to form groundwater that either overflows at the hillside foot (hillslope groundwater, HG) or percolates deep into the groundwater (depression groundwater, DG). The surface flow of the hillside unit (HS), combines with spring water and rainwater to form the depression surface water (DS). Subsequently, these surface waters migrate through the river channels of the watershed and ultimately reach the surface water outlet (OS). During this migration, surface water can exchange directly with depression groundwater (DG) through karst fractures. After combining with multiple depression surface waters, hillside springs, and rainwater sources, the mixed depression groundwater migrates through underground karst fracture pipes to the watershed's underground outlet (outlet groundwater, OG) (Chen et al., 2018; Zhang et al., 2019).

## 2.2. Sample collection and pretreatment

In the dry season (November to April), hillslope runoff and surface runoff are cut off, and 78.4% of water at the outlet of the watershed mainly comes from depression underground fracture flow (Zhang et al., 2019). In the rainy season (May to October), the hydrological outflow of the entire rainfall-runoff process can be more effectively traced. Therefore, multiple samples were collected in May, June, and September 2021 and July 2022 in this study.

The sample collection sites for observing hydrological processes are shown in Fig. 1c. Two Teflon boards were installed for collecting rainfall and throughfall samples as the method described in the previous study (Xia et al., 2021). Surface water samples in HS, DS, and OS were collected from hillslope runoff fields, the depression river channel, and the watershed surface water outlet point, respectively. Groundwater samples in HG, DG, and OG were collected from slope foot springs, observation wells, and the watershed groundwater outlet point, respectively.

At each observation point, water samples were collected and filtered through 0.7 μm quartz filters. The filters were pre-baked to remove Hg at high temperatures (480 °C) and then weighed before the filtration. After filtering, 4% (v/v) ultra-pure HCl and 5% (v/v) BrCl were added to the water samples. The dissolved Hg (DHg) was preconcentrated into a 40% mixed acid solution (v: v, HNO<sub>3</sub>: HCl=2:1) using the method established by Li et al. (2019). Due to the low concentrations of DHg (<1 ng/L) in this study, the volume of enriched samples needed to be > 15 L. Therefore, a 10 L bubble bottle was used to enrich Hg in the water sample twice into the same chlorinated activated carbon tube, and the enrichment flow rate was increased to 4 L/min. The whole process blank of the preconcentration was less than 0.4 ng. NIST RM 8610 standard

was added to the bubble bottle in the preconcentration unit to determine that no Hg isotope fractionation occurred during the process. The average recovery rate of the standard samples was 94% ± 2% (n = 3), and the average recovery rate of the water samples was 95% ± 5%.

The filters were freeze-dried and weighed to measure particulate Hg (PHg, ng/L) and the content of Hg per gram of particulate matter (Hg<sub>RSM</sub>). After weighing of filter samples, PHg was preconcentrated to 40% mixed acid solution (v: v, HNO<sub>3</sub>: HCl=2:1) using a tubular muffle furnace, as previously reported by Sun et al. (2013). To assess the data quality of the enrichment process, blank filters and certified reference material (GSS-4) were employed. The Hg content in the blank filter was less than 0.5 ng and the average recovery rate of the GSS-4 was 98% ± 7% (n = 5).

## 2.3. Hg concentration and isotope analyses

Analysis of DHg and PHg contents and isotopic compositions was performed at the State Key Laboratory of Environmental Geochemistry, Institute of Geochemistry, Chinese Academy of Sciences (CAS). Hg concentrations in the pretreated samples were determined by cold vapor atomic fluorescence spectrometry (CVAFS, Brooks Rand Model III) according to USEPA method 1631E (EPA, 2002). Hg isotopic compositions were measured using a Nu-Plasma II multi-collector inductively coupled plasma mass spectrometer (MC-ICP-MS) (Yin et al., 2010a). The uncertainty of Hg isotope compositions of CRMs is shown in Table S1. Based on the isotopic analysis precision of the MC-ICP-MS, the standard deviations (SD) for δ<sup>202</sup>Hg, Δ<sup>199</sup>Hg, Δ<sup>200</sup>Hg, and Δ<sup>201</sup>Hg were 0.10‰, 0.04‰, 0.04‰, and 0.04‰, respectively.

## 2.4. Multivariate mixing model of Hg isotope

If the Δ<sup>199</sup>Hg and Δ<sup>200</sup>Hg values of the receptor remain unaffected by fractionation processes, and there are significant variations in the Δ<sup>199</sup>Hg and Δ<sup>200</sup>Hg values among different end members, an isotopic ternary mixing model can be employed to estimate the quantitative contributions of different end members (f<sub>1</sub>, f<sub>2</sub>, f<sub>3</sub>) to Hg in the runoff water. The application of the model is as follows:

$$\Delta^{199}\text{Hg}_{\text{water-Hg}} = \Delta^{199}\text{Hg}_{f_1} \times f_1 + \Delta^{199}\text{Hg}_{f_2} \times f_2 + \Delta^{199}\text{Hg}_{f_3} \times f_3 \quad (1)$$

$$\Delta^{200}\text{Hg}_{\text{water-Hg}} = \Delta^{200}\text{Hg}_{f_1} \times f_1 + \Delta^{200}\text{Hg}_{f_2} \times f_2 + \Delta^{200}\text{Hg}_{f_3} \times f_3 \quad (2)$$

$$f_1 + f_2 + f_3 = 1 \quad (3)$$

Where f<sub>1</sub>, f<sub>2</sub>, and f<sub>3</sub> represent the estimated contributions from three end members (rainfall, deep soil, litterfall) in the runoff water. The isotopic data of deep soil and litterfall in this study area were adopted from Xia et al. (2020) (Table S4). Water<sub>Hg</sub> is either PHg or DHg in the runoff water. When Δ<sup>199</sup>Hg of water DHg is affected by some transformation process, it is corrected into Δ<sup>199</sup>Hg<sub>Sou-Mix</sub>, which is only affected by sources mixing. The DHg source mixing curve of the Chenqi watershed runoff was established in this study as follows, which was used in correcting Δ<sup>199</sup>Hg.

$$\Delta^{199}\text{Hg}_{\text{Sou-Mix}} = (2.36 \pm 1.70) \times \Delta^{200}\text{Hg}_{\text{waterDHg}} + (0.05 \pm 0.06) \quad (4)$$

The source mixing value of δ<sup>202</sup>Hg is defined as δ<sup>202</sup>Hg<sub>Sou-Mix</sub>, and it can be estimated by the following equation:

$$\delta^{202}\text{Hg}_{\text{Sou-Mix}} = \delta^{202}\text{Hg}_{f_1} \times f_1 + \delta^{202}\text{Hg}_{f_2} \times f_2 + \delta^{202}\text{Hg}_{f_3} \times f_3 \quad (5)$$

E<sup>199</sup>Hg and ε<sup>202</sup>Hg are defined by the following formulas:

$$E^{199}\text{Hg} = \Delta^{199}\text{Hg}_{\text{Act}} - \Delta^{199}\text{Hg}_{\text{Sou-Mix}} \quad (6)$$

$$\epsilon^{202}\text{Hg} = \delta^{202}\text{Hg}_{\text{Act}} - \delta^{202}\text{Hg}_{\text{Sou-Mix}} \quad (7)$$

Where Δ<sup>199</sup>Hg<sub>Act</sub> and δ<sup>202</sup>Hg<sub>Act</sub> refer to the actual measured value of the sample. E<sup>199</sup>Hg and ε<sup>202</sup>Hg are used to indicate the actual

enrichment characteristics of the Hg isotope due to multiple fractionation processes. All calculations were performed by Monte Carlo simulation in R language to obtain a more accurate mean and standard deviation (Text S1).

### 3. Results and discussion

#### 3.1. Hg content and isotope composition

The mean concentrations of DHg in rainfall, throughfall, and HS were  $4.91 \pm 2.41$  ng/L ( $\pm 1SD$ ) ( $n = 6$ ),  $5.92 \pm 2.12$  ng/L ( $n = 7$ ), and  $5.73 \pm 4.43$  ng/L ( $n = 8$ ), respectively, which were significantly higher than those in other surface runoffs ( $2.56 \pm 1.21$  ng/L,  $n = 9$ , average from DS and OS) and subsurface runoff ( $2.01 \pm 1.30$  ng/L,  $n = 29$ , average from HG, DG, and OG) (Fig. 2a, Table S2). The DHg concentrations were consistent with the values observed in natural waters that are not polluted or impacted by agricultural and urban activities in previous studies (Fu et al., 2010; Huang et al., 2015; Huang et al., 2012; Lyons et al., 2006; Zhang et al., 2020a; Zhao et al., 2017). In contrast to DHg, the concentrations of PHg showed comparable values ( $P > 0.05$ ) between different runoff observation points (Fig. 2b, Table S3), with total values ranging from 0.08 to 23.0 ng/L and a median of 1.42 ng/L. Some exceptionally high values were recorded, but the overall level was similar to those found in the Tibetan Plateau Basin and China's estuarine regions (Li et al., 2022; Lim et al., 2019; Liu et al., 2022). The correlation between DHg and PHg in the watersheds was not significant (Fig S1a),

and the average ratio of DHg to the sum of PHg and DHg was  $61.0 \pm 26.9\%$ . The content of Hg per gram of particulate matter ( $Hg_{RSM}$ , ng/g) in water bodies showed significantly higher values in open rainfall ( $402 \pm 29.4$  ng/g) and HG ( $311 \pm 144$  ng/g) than DG ( $92.8 \pm 74.7$  ng/g) (Fig S1b).  $Hg_{RSM}$  concentrations in runoff waters were generally higher than Hg concentrations in watershed soils ( $83.2 \pm 36.0$  ng/g) (Table S4), because other major constituents of terrestrial sources washed into the water body are more susceptible than dissolution of soil Hg (Jeandel and Oelkers, 2015).

The isotopic compositions of DHg in rainfall derived from open precipitation in the watershed area (Fig. 2c, d) showed higher  $\delta^{202}Hg$ ,  $\Delta^{199}Hg$ , and  $\Delta^{200}Hg$  values ( $\delta^{202}Hg$ :  $-1.04 \pm 0.51\%$ ,  $\Delta^{199}Hg$ :  $0.55 \pm 0.33\%$ , and  $\Delta^{200}Hg$ :  $0.19 \pm 0.10\%$ ) compared to those in Guiyang City ( $\delta^{202}Hg$ :  $-1.30 \pm 0.58\%$ ,  $\Delta^{199}Hg$ :  $0.39 \pm 0.17\%$ , and  $\Delta^{200}Hg$ :  $0.07 \pm 0.17\%$ ) (Yuan et al., 2018).  $\delta^{202}Hg$  and  $\Delta^{199}Hg$  values were lower, while  $\Delta^{200}Hg$  values were higher when compared with the data in Lhasa, China ( $\delta^{202}Hg$ :  $-0.80 \sim -0.42\%$ ,  $\Delta^{199}Hg$ :  $0.38 \sim 0.76\%$ ,  $\Delta^{200}Hg$ :  $0.10 \sim 0.15\%$ ) (Yuan et al., 2015). It appears that the isotopic composition of rainfall DHg in the study area was intermediate between urban and background areas.

The isotopic compositions of DHg in surface water ( $\delta^{202}Hg$ :  $-1.79 \pm 1.01\%$ ,  $\Delta^{199}Hg$ :  $0.23 \pm 0.19$ , and  $\Delta^{200}Hg$ :  $0.07 \pm 0.14\%$ ) and in groundwater ( $\delta^{202}Hg$ :  $-2.20 \pm 1.24\%$ ,  $\Delta^{199}Hg$ :  $0.06 \pm 0.09\%$ , and  $\Delta^{200}Hg$ :  $0.01 \pm 0.03\%$ ) showed much lower values relative to DHg in rainfall. The data were derived from multiple samples collected at various times, leading to large standard errors in the isotopic signatures.

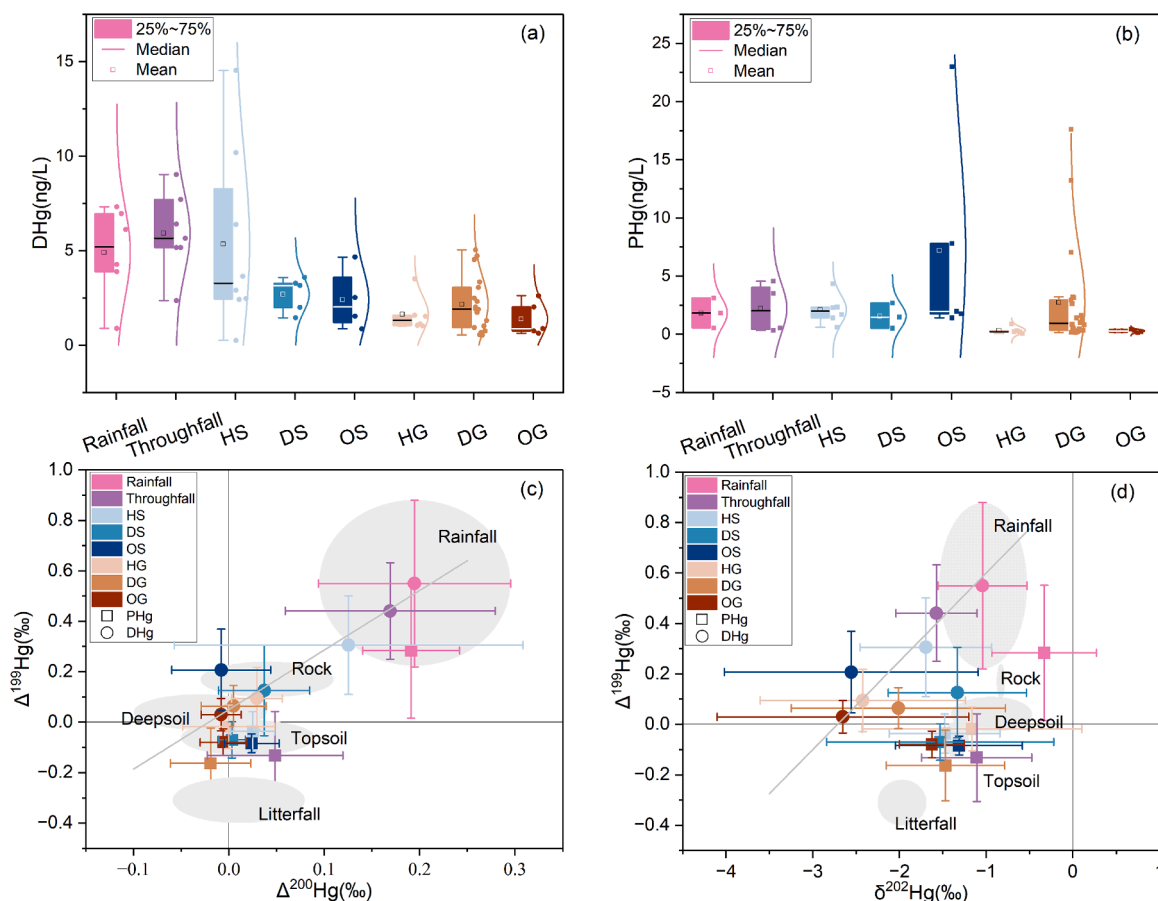


**Fig. 2.** Hg Concentration and Isotopic Composition of Water Samples in Rainfall-Runoff Processes. Panels (a) and (b) display the Hg concentrations of water samples from various sites, with each site's data presented in box plots accompanied by normal distribution curves. Panels (c) and (d) display the Hg isotopic composition of water samples (mean  $\pm 1$  standard deviation) at different sites. Terrestrial Hg isotopic compositions in the Chenqi watershed were adopted from Xia (2020), which are shown as ovals on this graph, representing 1-SD error ellipses around the mean. The gray line in panel (c) was the linear fitting curve of the values ( $\Delta^{199}Hg$  vs  $\Delta^{200}Hg$ ) of Rainfall, HS, DS, HG, DG, and OG. The gray line in panel (d) was the linear fitting curve of the values ( $\Delta^{199}Hg$  vs  $\delta^{202}Hg$ ) of Rainfall, HS, HG, and OG. Linear fittings were conducted using the York regression method in Origin Lab.

The large variability in rainfall Hg isotopic characteristics at different times was one reason for this. Additionally, factors such as the flow of runoff, ambient temperature, and soil humidity varying over time contributed to the variability at the same runoff site (Tsui et al., 2020). While the Hg isotopic composition of runoff at one site exhibited large variability and resulted in a large standard error, runoff Hg isotopic signatures at different sites revealed regular changes driven by runoff migration. The  $\Delta^{199}\text{Hg}$  and  $\Delta^{200}\text{Hg}$  values of DHg in both surface water and groundwater were distributed between those of rainfall and terrestrial sources (Fig. 2c). In the migration pathways of both surface and groundwater, the isotopic compositions of DHg gradually approached terrestrial sources in the order of hillslope, depression, and outlet. The  $\delta^{202}\text{Hg}$  values of DHg in runoff water (Fig. 2d) were significantly lower than those of terrestrial sources and rainfall.

The isotopic compositions of PHg in the watershed runoff water (Fig. 2c, d) ( $\delta^{202}\text{Hg}$ :  $-1.43 \pm 0.75\%$ ,  $\Delta^{199}\text{Hg}$ :  $-0.09 \pm 0.11\%$ , and  $\Delta^{200}\text{Hg}$ :  $-0.01 \pm 0.04\%$ ) were distributed between those of deep soil and litterfall. They were similar to those of the topsoil of the watershed, and only the  $\Delta^{199}\text{Hg}$  of PHg in the depression groundwater (DG) was significantly negative. The differences in  $\Delta^{200}\text{Hg}$  of PHg between different runoff waters were not insignificant. However, it can be seen that the closer to the surface and the rainfall, the more positive  $\Delta^{200}\text{Hg}$  values of PHg were observed in the runoff waters.

### 3.2. Mass-independent fractionation

More details about runoff processes were revealed by our systematic observation than those in previous studies (Oswald et al., 2014; Yuan et al., 2024). In the  $\Delta^{199}\text{Hg}$ - $\Delta^{200}\text{Hg}$  mapping (Fig. 2c), the DHg isotopes in all runoff waters (except the OS) were located on the same straight line with rainfall. It was demonstrated that in both surface and subsurface pathways, as runoff migrated farther away, the MIF signals of DHg in runoff water were closer to terrestrial sources and farther away from rainfall. The phenomenon that  $\Delta^{199}\text{Hg}$  of runoff DHg distributed on a straight line is consistent with the variation of  $\Delta^{200}\text{Hg}$ . There are two possible reasons for this phenomenon: 1) the  $\Delta^{199}\text{Hg}$  as well as  $\Delta^{200}\text{Hg}$  in the runoff DHg were driven only by the mixing of the sources, and 2)  $\Delta^{199}\text{Hg}$  was driven by some transformation processes of the DHg in the water body to become progressively negative during migration. It is unlikely that the processes causing MIF can simultaneously influence the occurrence of regular changes in runoff across different sites with varying environmental conditions, such as oxic or anoxic, and light or dark settings (Motta et al., 2020; Schwab et al., 2023; Zheng and Hintelmann, 2010b). The fitted straight line " $y = (2.36 \pm 1.70)x + (0.05 \pm 0.06)$ " in the  $\Delta^{199}\text{Hg}$ - $\Delta^{200}\text{Hg}$  mapping (Fig. 2c) was interpreted as the DHg source mixing curve of the watershed runoff.

The  $\Delta^{199}\text{Hg}$  values of DHg in OS diverged towards positive from the source mixing curve (Fig. 2c). Considering that there were no other exogenous inputs to OS, in addition to different source mixing, DHg in OS may have undergone photochemical reduction which will result in positive odd-MIF. The  $\Delta^{199}\text{Hg}_{\text{Sou-Mix}}$  value of OS ( $0.03 \pm 0.16\%$ ), which was only controlled by source mixing, can be calculated from its  $\Delta^{200}\text{Hg}$  value and the DHg source mixing curve. By establishing the DHg source mixing curve,  $\Delta^{200}\text{Hg}$  and  $\Delta^{199}\text{Hg}$  of DHg in runoff water can effectively serve as indicators for tracking the source of DHg in any watershed.

PHg of runoff water mainly consists of residues from dissolution or adsorption-precipitation processes (Sansalone and Kim, 2008; Viers et al., 2009), and terrestrial sources and water DHg can be interpreted as the main sources of PHg in water bodies. It is known that dissolution (Yin et al., 2013) and adsorption-precipitation processes do not produce MIF (Wiederhold et al., 2010),  $\Delta^{199}\text{Hg}$  and  $\Delta^{200}\text{Hg}$  of particulate matter in runoff are also effective indicators for tracking PHg sources.

### 3.3. Quantitative sources contribution to runoff Hg

DHg in runoff water originates from the mixing of rainfall Hg and terrestrial Hg, with the latter entering the dissolved component through dissolution processes, which does not generate MIF (Jiskra et al., 2012; Yin et al., 2013). Topsoil is usually used directly as the contributing end member of terrestrial Hg in the Hg isotope mixing model in the background area (Woernle et al., 2018; Xia et al., 2022; Zhang et al., 2020b). However, our data showed that the topsoil was not on the source mixing curve of DHg from rainfall-runoff in the watershed. This may be because multiple terrestrial sources of Hg, such as deep soil, topsoil, litterfall, and bedrock, all contributed to DHg in the water body. Previous studies classified the contributing end members of topsoil Hg as rainfall, litterfall, and rock weathering (Gao et al., 2023; Liu et al., 2022; Wang et al., 2017). In this study, after analyzing the isotopic composition of all terrestrial sources of Hg in the watershed, we found that the Hg isotopic signals ( $\Delta^{199}\text{Hg}$ ,  $\Delta^{200}\text{Hg}$ ,  $\delta^{202}\text{Hg}$ ) in the topsoil could be explained as a mixture of deep soil, rainfall, and litterfall (Fig. 2c, 2d). And considering the small contribution of bedrock Hg to runoff, deep soil and litterfall can be specified as the terrestrial Hg contribution end members in the watershed.

Water PHg is derived from the water DHg and terrestrial sources of Hg in the watershed. Since the MIF values of water DHg were only controlled by source mixing, except for surface water outlet (OS), the sources of PHg for these runoff waters can be similarly substituted by deep soil, litterfall, and rainfall.

As mentioned above, a ternary mixing model can be used to quantify the contributions of different sources to runoff Hg during hydrologic processes. The sources of DHg in OS were calculated using  $\Delta^{199}\text{Hg}_{\text{Sou-Mix}}$ , which was corrected by the watershed source mixing curve. Moreover, the high total suspended solids content in OS (median = 23.2 mg/L, Table S3) suggested that its PHg may be predominantly influenced by land-based Hg sources, which can be directly assumed as its PHg source. The result of Hg source quantification for all runoff waters is presented in Fig. 3.

The percentage contributions of DHg sources showed significant variations (Fig. 3a, Table S5). When water migrated over land surface, the proportion of rainfall-sourced Hg in the runoff water gradually decreased from  $42.1 \pm 20.6\%$  in HS to  $17.3 \pm 11.4\%$  in OG, indicating that the DHg in the runoff water was increasingly impacted by terrestrial sources. In both surface and groundwater migration pathways, it was observed that the longer the migration time, the greater the contribution of terrestrial sources to DHg. In groundwater runoff migration, the percentage contribution of litterfall to Hg remained relatively stable (from  $29.8 \pm 18.4\%$  to  $31.7 \pm 19.4\%$ ), while the contribution of deep soil increased from  $42.9 \pm 22.1\%$  to  $52.2 \pm 22.0\%$ . Conversely, for surface runoff migration, the contributions of litterfall and deep soil to DHg gradually increased. By examining the distribution of DHg from various sources during the hydrological process (Fig. 3c, Table S5), it was found that Hg from rainfall sources was adsorbed on the land surface, leading to a gradual decrease in its contribution to the water body. This finding was consistent with previous results from isotope addition experiments, suggesting the newly deposited Hg was more readily preserved on the terrestrial surface (Oswald et al., 2014; Yuan et al., 2024). Hg concentration from terrestrial sources did not show an increase in the depression area of this watershed. This may be because changes in soil type, land use, and vegetation cover in this watershed did not significantly affect runoff Hg. Terrestrial sources of Hg in the generation area were the primary source of runoff DHg in this watershed.

PHg in water bodies also showed a gradually decreasing contribution of rainfall-derived Hg with runoff migration (Fig. 3b). In the surface runoff migration pathway, the change of  $\text{Hg}_{\text{RSM}}$  with migration processes was opposite to that of DHg (Fig. 3c, d, HS-DS-OS), which may correspond to the partitioning of Hg between dissolved and particulate phases in the water body. PHg in the groundwater migration pathway showed different variations to surface water. The amount of PHg from

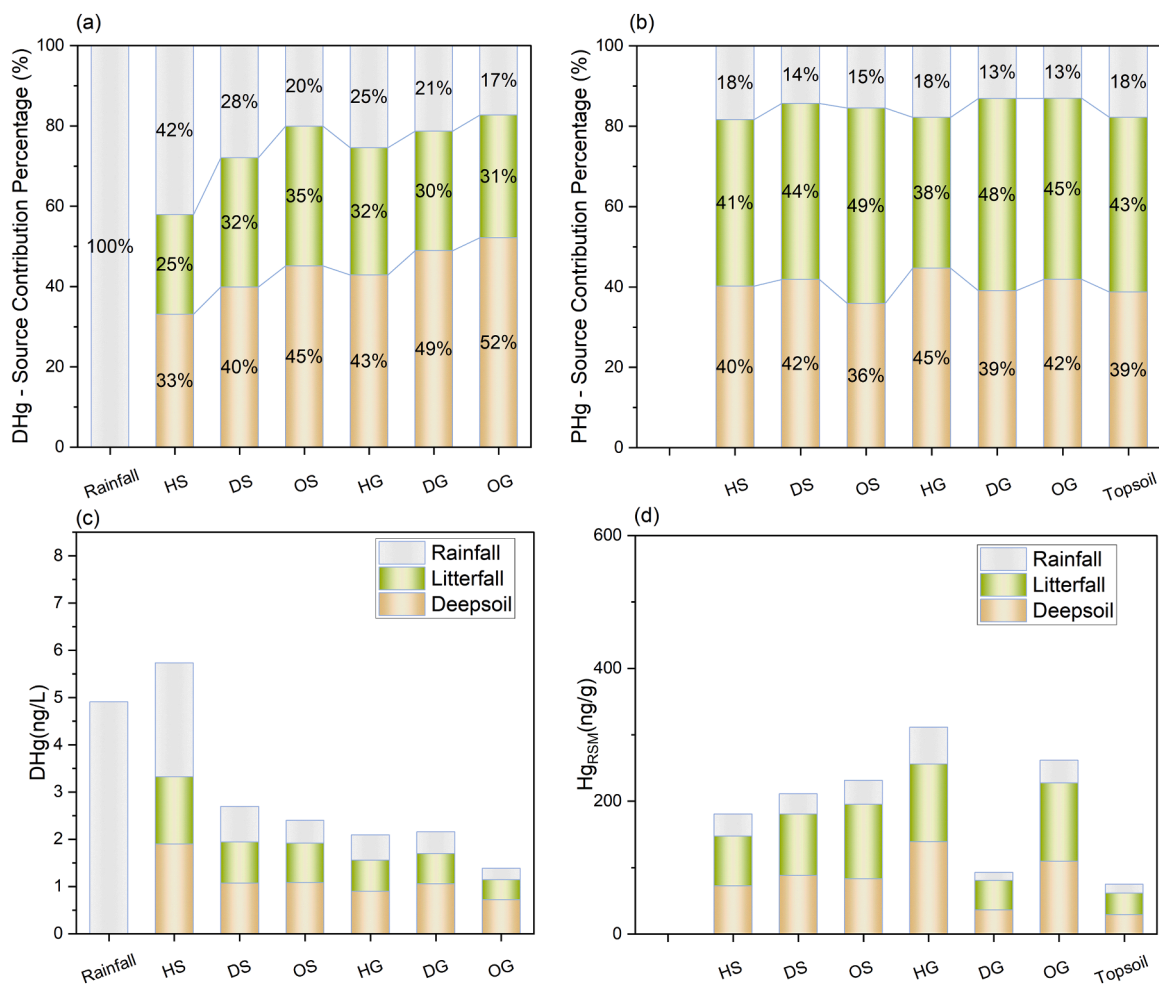


Fig. 3. Contribution of Different Sources and Hg Concentrations in Runoff Water during Hydrological Process. Panels (a) and (c) display source contribution changes of dissolved Hg (DHg) at various runoff sites. Panels (b) and (d) display source contribution changes of particulate Hg (PHg) at various runoff sites. Hg<sub>RSM</sub> denotes Hg content per gram of particulate matter in runoff water.

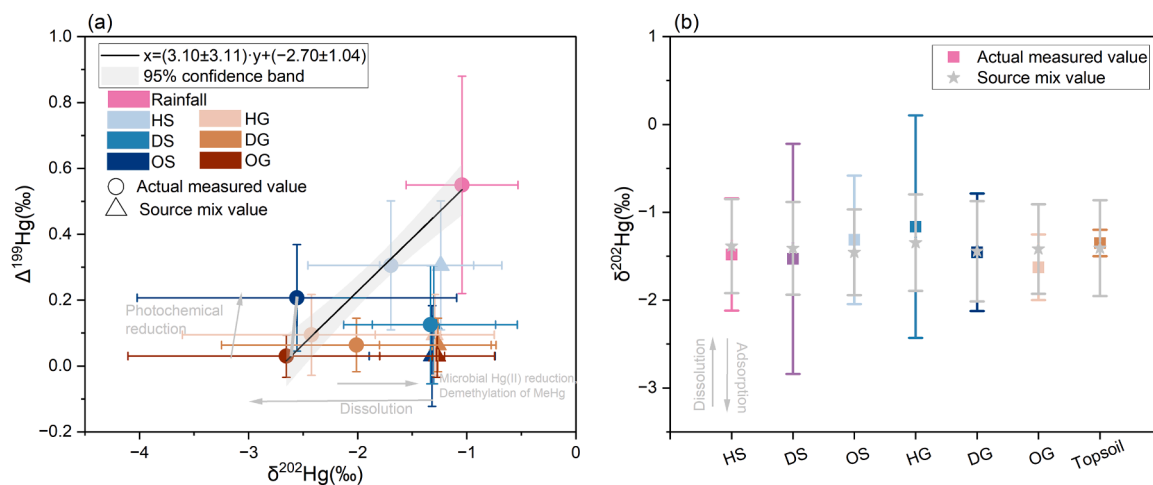


Fig. 4. Comparison of the Actual Measured Isotopic Signals with the Source Mixing Values. (a) Comparison of the actual measured values of the DHg isotopic signals with the source mixing values ( $\Delta^{199}\text{Hg}_{\text{Sou-Mix}}$ ,  $\delta^{202}\text{Hg}_{\text{Sou-Mix}}$ ). Data are shown as the mean  $\pm$  1 standard deviation. The gray line in panel (a) was the linear fitting curve of  $\Delta^{199}\text{Hg}$  and  $\delta^{202}\text{Hg}$  in Rainfall, HS, HG, and OG (by York regression method in Origin Lab). For sites where the actual measured values aligned with the fitted line, Hg isotope in DHg was dominantly impacted by the dissolution-adsorption process. (b) Comparison of the actual measured values of the PHg isotopic signals with the source mixing values ( $\delta^{202}\text{Hg}_{\text{Sou-Mix}}$ ). Data are shown as the mean  $\pm$  1 standard deviation. Dissolution promotes a positive  $\delta^{202}\text{Hg}$  shift in PHg compared to the source mixing, while adsorption causes a negative shift.

land sources gradually increases in surface water, while it decreases in groundwater.

### 3.4. Key processes driving runoff Hg transformation

The  $\Delta^{199}\text{Hg}-\delta^{202}\text{Hg}$  mapping of DHg (Fig. 4a) showed that rainfall, HS, HG, and OG all changed along a straight line. Compared to the  $\delta^{202}\text{Hg}_{\text{Sou-mix}}$  of these runoffs, the actual  $\delta^{202}\text{Hg}$  values of DHg at runoff sites on this line were more negative. The analysis of MIF data in runoff DHg in Section 3.2 has shown that these runoffs did not experience transformation processes that would affect the MIF, except for OS. There must be a widespread transformation process in HS, HG, and OG, which resulted in a negative MDF and no change in MIF for the runoff DHg, and it allowed us to observe this straight line. The most plausible explanation for this transformation process is the dissolution and adsorption of Hg (Broczka et al., 2019; Wiederhold et al., 2010; Yin et al., 2013). The presence of DHg in water bodies is a result of the interaction between dissolved Hg from terrestrial sources entering the water runoff and adsorbed terrestrial substances leaving the water body. As the degree of dissolution increases, the value of  $\epsilon^{202}\text{Hg}$  in water DHg also changes linearly (Broczka et al., 2019). The DHg of these runoff points on the line is mainly driven by dissolution and adsorption processes. This curve ( $\delta^{202}\text{Hg} = (3.10 \pm 3.11) \Delta^{199}\text{Hg} + (-2.70 \pm 1.04)$ ) can be referred to as the dissolved adsorption effect line for runoff DHg in this watershed.

For runoff sites not located on the line, the  $\epsilon^{202}\text{Hg}$  was the result of the combined effects of dissolution, adsorption, and other transformation processes. The  $\epsilon^{202}\text{Hg}_{\text{dissolution-adsorption}}$  led by the Hg dissolution and adsorption process for the runoff can be determined from the dissolved adsorption effect line. The variances of  $\epsilon^{202}\text{Hg}$  and  $\epsilon^{202}\text{Hg}_{\text{dissolution-adsorption}}$  represent the  $\epsilon^{202}\text{Hg}_{\text{other-process}}$  led by other transformation processes (Table S6). We can use  $\epsilon^{202}\text{Hg}$  and  $E^{199}\text{Hg}$  of these runoff sites to determine other transformation processes that occurred. The other transformation processes of DHg in DG and DS did not cause significant MIF but led to a positive MDF, which is similar to the isotope shift via microbial Hg(II) reduction (Kritee et al., 2007) and demethylation of MeHg (Kritee et al., 2009). The  $\epsilon^{202}\text{Hg}$  was estimated to be  $-1.27 \pm 1.19\%$  during the dissolution-adsorption process and  $0.51 \pm 1.64\%$  during the other process in DG. Correspondingly, the values were  $-1.05 \pm 1.39\%$  and  $1.03 \pm 1.51\%$  in the DS. As previously reported, a large amount of surface water is stored in paddy fields during the rice growing season, and exchange between surface and groundwater in depressions occurs (Zhang et al., 2019; 2020b). Waterlogged fields may provide anoxic and organic-rich environments for microorganisms to reduce DHg in depression runoff (Lu et al., 2016; Zheng et al., 2012).

The transformation processes of DHg in OS water resulted in  $E^{199}\text{Hg}$  of  $0.18 \pm 0.22\%$ . The dissolution-adsorption process caused  $\epsilon^{202}\text{Hg}$  of  $-1.30 \pm 1.31\%$ , and other processes led to  $\epsilon^{202}\text{Hg}$  of  $0.06 \pm 1.88\%$ . These values are similar to the slope of the  $\Delta^{199}\text{Hg}/\delta^{202}\text{Hg}$  line in the photochemical reduction process (Bergquist and Blum, 2007; Blum et al., 2014; Zheng and Hintelmann, 2010a), indicating that the photochemical reduction was also a driving process of DHg in OS, in addition to the dissolution and adsorption process.

Throughout the runoff migration process, the dissolution effect was consistently greater than the adsorption effect, and the difference between the two increased gradually over time (Fig. 4a), which explained the observed gradual increase in the contribution of terrestrial Hg to DHg in runoff waters. The  $\epsilon^{202}\text{Hg}$  resulted from the dissolution-adsorption processes varied from  $-0.37 \pm 0.70\%$  to  $-1.38 \pm 1.54\%$ . In paddy fields, in addition to dissolution and adsorption, microbial Hg (II) reduction and demethylation of MeHg result in DHg in runoff water being reduced into the atmosphere, as seen in DG and DS. Furthermore, in water bodies with low water exchange rates and large surface areas, like OS in this study, photochemical reduction plays a significant role in driving Hg emissions to the atmosphere.

For PHg,  $\epsilon^{202}\text{Hg}$  is mainly caused by both dissolution and adsorption processes. Dissolution promotes a more positive  $\delta^{202}\text{Hg}$  of PHg

compared to the source mixing, while the dissolved Hg component adsorbed in the particle phase causes a more negative  $\delta^{202}\text{Hg}$  of PHg. The more positive  $\epsilon^{202}\text{Hg}$  indicates a stronger dissolution than the adsorption effect. In HG and OS, the  $\epsilon^{202}\text{Hg}$  values of PHg were positive, mainly due to the dissolved residues of terrestrial materials (Fig. 4b, Table S7). In HS, DS, DG, and OG, the  $\epsilon^{202}\text{Hg}$  values of PHg were negative, indicating that PHg in the water body is controlled mainly by the adsorption process. This suggests that PHg in groundwater underwent a transformation process from terrestrial dissolved residues to runoff Hg as reprecipitation products. PHg in surface water was directly washed into the water body from land-based materials and then gradually changed into dissolved form. PHg in groundwater was controlled by its underground residence time, while PHg in surface runoff was mainly controlled by the flow rate of runoff.

## 4. Conclusion and implications

This study clarifies the ambiguity that existed in previous studies regarding the sources and dominant transformation processes of Hg in runoff water. The corrected  $\Delta^{199}\text{Hg}_{\text{Sou-Mix}}$  can be obtained from the DHg source mixing curve established by the  $\Delta^{200}\text{Hg}$ . Corrected  $\Delta^{199}\text{Hg}$  and  $\Delta^{200}\text{Hg}$  are proven as effective quantitative indicators for runoff Hg. The combined use of MDF and MIF visualizes the sources and transformations of runoff Hg during the rainfall-runoff process. In summary, DHg in the runoff water is the result of a combination of three processes: (i) the dissolution of terrestrial source Hg into the water column, (ii) the adsorption of aqueous Hg by land from the water column, and (iii) other processes that reduce DHg in water to the atmosphere. During the rainfall-runoff process, Hg from rainfall tends to be trapped on land by adsorption and dissolved terrestrial Hg tends to be the main source of runoff DHg downstream. For this watershed, the process of microbial Hg (II) reduction and demethylation of MeHg occurred for DHg in runoff water when the runoff flows through the paddy field. Photochemical reduction played a significant role in DHg transformation in the surface water outlet, which has low water exchange rates and large surface areas. PHg in runoff water had a similar isotopic composition to topsoil, and dissolution and adsorption were the dominant transformation processes. PHg was mainly controlled by runoff flow in surface water and subsurface residence time in groundwater. Further studies can expand the scope to large-scale watersheds or entire terrestrial ecosystems and waterbodies impacted by anthropogenic wastewater discharges, which can better understand runoff Hg contamination in the global Hg biogeochemical cycle.

### CRediT authorship contribution statement

**Ruolan Li:** Writing – review & editing, Writing – original draft, Methodology, Investigation. **Junyao Yan:** Writing – review & editing, Methodology, Investigation. **Chuan Wang:** Writing – review & editing, Methodology, Investigation. **Shaochen Yang:** Writing – review & editing, Methodology, Investigation. **Lin Zhang:** Methodology, Investigation. **Tao Peng:** Software, Methodology, Data curation. **Wei Zhu:** Writing – review & editing, Methodology. **Ping Li:** Writing – review & editing, Supervision, Methodology, Investigation, Funding acquisition, Data curation, Conceptualization. **Leiming Zhang:** Writing – review & editing, Methodology. **Xinbin Feng:** Writing – review & editing, Supervision, Methodology.

### Declaration of competing interest

The authors declare that they have no known competing financial interests or personal relationships that could have appeared to influence the work reported in this paper.

## Data availability

Data will be made available on request.

## Acknowledgement

This study was funded by the National Natural Science Foundation of China (41921004), the Strategic Priority Research Program of Chinese Academy of Sciences (XDB40020403), the CAS Interdisciplinary Innovation Team (JCTD-2020–20), Youth Innovation Promotion Association of Chinese Academy of Sciences (Y2021106), and Guizhou Provincial 2020 Science and Technology Subsidies (No. GZ2020SIG).

## Supplementary materials

Supplementary material associated with this article can be found, in the online version, at [doi:10.1016/j.watres.2024.122044](https://doi.org/10.1016/j.watres.2024.122044).

## References

- Aleku, D.L., Lazareva, O., Pichler, T., 2024. Mercury in Groundwater–Source, Transport and Remediation. *Appl. Geochem.*, 106060.
- Beckers, F., Rinklebe, J., 2017. Cycling of mercury in the environment: Sources, fate, and human health implications: A review. *Crit. Rev. Environ. Sci. Technol.* 47 (9), 693–794.
- Bergquist, B.A., Blum, J.D., 2007. Mass-dependent and -independent fractionation of Hg isotopes by photoreduction in aquatic systems. *Science* (1979) 318 (5849), 417–420.
- Bishop, K., Shanley, J.B., Riscassi, A., de Wit, H.A., Eklöf, K., Meng, B., Mitchell, C., Osterwalder, S., Schuster, P.F., Webster, J., Zhu, W., 2020. Recent advances in understanding and measurement of mercury in the environment: Terrestrial Hg cycling. *Sci. Total Environ.* 721, 137647.
- Blum, J.D., Sherman, L.S., Johnson, M.W., 2014. Mercury Isotopes in Earth and Environmental Sciences. *Annu Rev Earth Pl Sc* 42, 249–269.
- Broczka, F.M., Biester, H., Richard, J.H., Kraemer, S.M., Wiederhold, J.G., 2019. Mercury Isotope Fractionation in the Subsurface of a Hg(II) Chloride-Contaminated Industrial Legacy Site. *Environ. Sci. Technol.* 53 (13), 7296–7305.
- Cai, H.M., Chen, J.B., 2016. Mass-independent fractionation of even mercury isotopes. *Sci. Bull. (Beijing)* 61 (2), 116–124.
- Cao, L., Wang, S.J., Peng, T., Cheng, Q.Y., Zhang, L., Zhang, Z.C., Yue, F.J., Fryer, A.E., 2020. Monitoring of suspended sediment load and transport in an agroforestry watershed on a karst plateau, Southwest China. *Agriculture Ecosystems & Environment* 299, 106976.
- Chen, X., Zhang, Z.C., Soulsby, C., Cheng, Q.B., Binley, A., Jiang, R., Tao, M., 2018. Characterizing the heterogeneity of karst critical zone and its hydrological function: An integrated approach. *Hydrol. Process.* 32 (19), 2932–2946.
- Cheng, Q., Wang, S., Peng, T., Cao, L., Zhang, X., Buckerfield, S.J., Zhang, Y., Collins, A. L., 2020. Sediment sources, soil loss rates and sediment yields in a Karst plateau catchment in Southwest China. *Agriculture Ecosystems & Environment* 304, 107114.
- EPA, U., 2002. Method 1631, Revision E: Mercury in Water By oxidation, Purge and trap, and Cold Vapor Atomic Fluorescence Spectrometry. USEPA.
- Fu, X.W., Feng, X., Dong, Z.Q., Yin, R.S., Wang, J.X., Yang, Z.R., Zhang, H., 2010. Atmospheric gaseous elemental mercury (GEM) concentrations and mercury depositions at a high-altitude mountain peak in south China. *Atmospheric Chem. Phys.* 10 (5), 2425–2437.
- Gao, X., Yuan, W., Chen, J.B., Huang, F., Wang, Z.R., Gong, Y.F., Zhang, Y.M., Liu, Y., Zhang, T., Zheng, W., 2023. Tracing the source and transport of Hg during pedogenesis in strongly weathered tropical soil using Hg isotopes. *Geochim. Cosmochim. Acta* 361, 101–112.
- Gao, Z.Y., Li, M.M., Wang, J., Yan, J., Zhou, C.C., Yan, C.H., 2018. Blood mercury concentration, fish consumption and anthropometry in Chinese children: A national study. *Environ. Int.* 110, 14–21.
- Gebka, K., Beldowska, M., Szymczak, E., Saniewska, D., 2019. Temporal changes in the content of labile and stable mercury forms in soil and their inflow to the southern Baltic Sea. *Ecotoxicol. Environ. Saf.* 182, 109434.
- Gebka, K., Saniewska, D., Beldowska, M., 2020. Mobility of mercury in soil and its transport into the sea. *Environ. Sci. Pollut. Res.* 27 (8), 8492–8506.
- Gong, Y., Chen, X., Zhang, Z., Zhang, R., Cheng, Q., 2019. Analysis of flood lag time and similarity in small karst peak cluster-depression watersheds. *Advances in Science and Technology of Water Resources* 39 (4), 7–12.
- Huang, J., Kang, S.C., Zhang, Q.G., Guo, J.M., Sillanpää, M., Wang, Y.J., Sun, S.W., Sun, X.J., Tripathee, L., 2015. Characterizations of wet mercury deposition on a remote high-elevation site in the southeastern Tibetan Plateau. *Environ. Pollut.* 206, 518–526.
- Huang, J., Kang, S.C., Zhang, Q.G., Yan, H.Y., Guo, J.M., Jenkins, M.G., Zhang, G.S., Wang, K., 2012. Wet deposition of mercury at a remote site in the Tibetan Plateau: Concentrations, speciation, and fluxes. *Atmos. Environ.* 62, 540–550.
- Jeandel, C., Oelkers, E.H., 2015. The influence of terrigenous particulate material dissolution on ocean chemistry and global element cycles. *Chem. Geol.* 395, 50–66.
- Jiskra, M., Wiederhold, J.G., Bourdon, B., Kretzschmar, R., 2012. Solution Speciation Controls Mercury Isotope Fractionation of Hg(II) Sorption to Goethite. *Environ. Sci. Technol.* 46 (12), 6654–6662.
- Kritee, K., Barkay, T., Blum, J.D., 2009. Mass dependent stable isotope fractionation of mercury during mer mediated microbial degradation of monomethylmercury. *Geochim. Cosmochim. Acta* 73 (5), 1285–1296.
- Kritee, K., Blum, J.D., Johnson, M.W., Bergquist, B.A., Barkay, T., 2007. Mercury stable isotope fractionation during reduction of Hg (II) to Hg (0) by mercury resistant microorganisms. *Environ. Sci. Technol.* 41 (6), 1889–1895.
- Li, K., Lin, C.J., Yuan, W., Sun, G.Y., Fu, X.W., Feng, X.B., 2019. An improved method for recovering and preconcentrating mercury in natural water samples for stable isotope analysis. *J. Anal. At. Spectrom.* 34 (11), 2303–2313.
- Li, Y., Yan, H., Rong, Y., Lin, J., Xue, W., 2022. The distribution characteristics of mercury species in the estuaries of the ten main rivers in China and flux of mercury from rivers to the ocean. *Acta Scientiae Circumstantiae* 42 (10), 323–331.
- Lim, A.G., Sonke, J.E., Krickov, I.V., Manasyapov, R.M., Loiko, S.V., Pokrovsky, O.S., 2019. Enhanced particulate Hg export at the permafrost boundary, western Siberia. *Environ. Pollut.* 254, 113083.
- Liu, J.L., Xu, X.R., Yu, S., Cheng, H., Peng, J.X., Hong, Y.G., Feng, X.B., 2014. Mercury contamination in fish and human hair from Hainan Island, South China Sea: Implication for human exposure. *Environ. Res.* 135, 42–47.
- Liu, N.T., Wu, F., Yuan, W., Wang, X., Wang, D.Y., 2022. Mercury Speciation, Distribution, and Potential Sources in Surface Waters of the Yangtze and Yellow River Source Basins of Tibetan Plateau During Wet Season. *Environmental Science* 43 (11), 5064–5072.
- Lu, X., Liu, Y., Johs, A., Zhao, L., Wang, T., Yang, Z., Lin, H., Elias, D.A., Pierce, E.M., Liang, L., 2016. Anaerobic mercury methylation and demethylation by *Geobacter bemedjensis* Bem. *Environ. Sci. Technol.* 50 (8), 4366–4373.
- Luo, H., Cheng, Q., Pan, X., 2020. Photochemical behaviors of mercury (Hg) species in aquatic systems: a systematic review on reaction process, mechanism, and influencing factor. *Sci. Total Environ.* 720, 137540.
- Lyons, W.B., Fitzgibbon, T.O., Welch, K.A., Carey, A.E., 2006. Mercury geochemistry of the Scioto River, Ohio: Impact of agriculture and urbanization. *Appl. Geochem.* 21 (11), 1880–1888.
- Motta, L.C., Kritee, K., Blum, J.D., Tsui, M.T.K., Reinfelder, J.R., 2020. Mercury Isotope Fractionation during the Photochemical Reduction of Hg(II) Coordinated with Organic Ligands. *J. Phys. Chem. A* 124 (14), 2842–2853.
- Obriest, D., Kirk, J.L., Zhang, L., Sunderland, E.M., Jiskra, M., Selin, N.E., 2018. A review of global environmental mercury processes in response to human and natural perturbations: Changes of emissions, climate, and land use. *Ambio* 47 (2), 116–140.
- Oswald, C.J., Heyes, A., Branfreun, B.A., 2014. Fate and Transport of Ambient Mercury and Applied Mercury Isotope in Terrestrial Upland Soils: Insights from the METAALICUS Watershed. *Environ. Sci. Technol.* 48 (2), 1023–1031.
- Qiao, P., Wang, S., Li, J., Zhao, Q., Wei, Y., Lei, M., Yang, J., Zhang, Z., 2023. Process, influencing factors, and simulation of the lateral transport of heavy metals in surface runoff in a mining area driven by rainfall: A review. *Sci. Total Environ.* 857, 159119.
- Rodríguez-González, P., Epov, V.N., Bridou, R., Tessier, E., Guyoneaud, R., Monperrus, M., Amouroux, D., 2009. Species-specific stable isotope fractionation of mercury during Hg (II) methylation by an anaerobic bacteria (*Desulfobulbus propionicus*) under dark conditions. *Environ. Sci. Technol.* 43 (24), 9183–9188.
- Sansalone, J.J., Kim, J.Y., 2008. Suspended particle destabilization in retained urban stormwater as a function of coagulant dosage and redox conditions. *Water. Res.* 42 (4–5), 909–922.
- Schwab, L., Gallati, N., Reiter, S.M., Kimber, R.L., Kumar, N., McLagan, D.S., Biester, H., Kraemer, S.M., Wiederhold, J.G., 2023. Mercury Isotope Fractionation during Dark Abiotic Reduction of Hg(II) by Dissolved, Surface-Bound, and Structural Fe(II). *Environ. Sci. Technol.* 57 (40), 15243–15254.
- Sun, R., Enrico, M., Heimbürger, L.E., Scott, C., Sonke, J.E., 2013. A double-stage tube furnace—acid-trapping protocol for the pre-concentration of mercury from solid samples for isotopic analysis. *Anal. Bioanal. Chem.* 405, 6771–6781.
- Sun, T., Ma, M., Wang, X., Wang, Y., Du, H., Xiang, Y., Xu, Q., Xie, Q., Wang, D., 2019. Mercury transport, transformation and mass balance on a perspective of hydrological processes in a subtropical forest of China. *Environ. Pollut.* 254, 113065.
- Tsui, M.T.K., Uzun, H., Ruecker, A., Majidzadeh, H., Ulus, Y., Zhang, H., Bao, S., Blum, J. D., Karanfil, T., Chow, A.T., 2020. Concentration and isotopic composition of mercury in a blackwater river affected by extreme flooding events. *Limnol. Oceanogr.* 65 (9), 2158–2169.
- Viers, J., Dupré, B., Gaillardet, J., 2009. Chemical composition of suspended sediments in World Rivers: New insights from a new database. *Sci. Total Environ.* 407 (2), 853–868.
- Wang, X., Luo, J., Yin, R.S., Yuan, W., Lin, C.J., Sommar, J., Feng, X.B., Wang, H.M., Lin, C., 2017. Using Mercury Isotopes To Understand Mercury Accumulation in the Montane Forest Floor of the Eastern Tibetan Plateau. *Environ. Sci. Technol.* 51 (2), 801–809.
- Wang, X., Yuan, W., Lin, C.J., Feng, X., 2022. Mercury cycling and isotopic fractionation in global forests. *Crit. Rev. Environ. Sci. Technol.* 52 (21), 3763–3786.
- Wiederhold, J.G., Cramer, C.J., Daniel, K., Infante, I., Bourdon, B., Kretzschmar, R., 2010. Equilibrium Mercury Isotope Fractionation between Dissolved Hg(II) Species and Thiol-Bound Hg. *Environ. Sci. Technol.* 44 (11), 4191–4197.
- Woerdle, G.E., Tsui, M.T.K., Sebestyen, S.D., Blum, J.D., Nie, X.P., Kolka, R.K., 2018. New Insights on Ecosystem Mercury Cycling Revealed by Stable Isotopes of Mercury in Water Flowing from a Headwater Peatland Catchment. *Environ. Sci. Technol.* 52 (4), 1854–1861.
- Xia, J., 2020. Biogeochemical Cycling and Mass Balance of Mercury in Typical Karst Catchment in Guizhou province. The University of Chinese Academy of Sciences.

- Xia, J., Wang, J., Zhang, L., Wang, X., Yuan, W., Anderson, C.W., Chen, C., Peng, T., Feng, X., 2021. Significant mercury efflux from a Karst region in Southwest China—Results from mass balance studies in two catchments. *Sci. Total Environ.* 769, 144892.
- Xia, J.C., Wang, J.X., Zhang, L.M., Wang, X., Yuan, W., Peng, T., Zheng, L.R., Tian, W.J., Feng, X.B., 2022. Migration and transformation of soil mercury in a karst region of southwest China: Implications for groundwater contamination. *Water Res.* 226, 119271.
- Yin, R.S., Feng, X.B., Foucher, D., Shi, W.F., Zhao, Z.Q., Wang, J., 2010a. High Precision Determination of Mercury Isotope Ratios Using Online Mercury Vapor Generation System Coupled with Multicollector Inductively Coupled Plasma-Mass Spectrometer. *Chinese Journal of Analytical Chemistry* 38 (7), 929–934.
- Yin, R., Feng, X., Shi, W., 2010b. Application of the stable-isotope system to the study of sources and fate of Hg in the environment: A review. *Appl. Geochem.* 25 (10), 1467–1477.
- Yin, R.S., Feng, X.B., Wang, J.X., Bao, Z.D., Yu, B., Chen, J.B., 2013. Mercury isotope variations between bioavailable mercury fractions and total mercury in mercury contaminated soil in Wanshan Mercury Mine, SW China. *Chem. Geol.* 336, 80–86.
- Yuan, S.L., Chen, J.B., Cai, H.M., Yuan, W., Wang, Z.W., Huang, Q., Liu, Y.J., Wu, X.Y., 2018. Sequential samples reveal significant variation of mercury isotope ratios during single rainfall events. *Sci. Total Environ.* 624, 133–144.
- Yuan, S.L., Zhang, Y.Y., Chen, J.B., Kang, S.C., Zhang, J., Feng, X.B., Cai, H.M., Wang, Z. H., Wang, Z.W., Huang, Q., 2015. Large variation of mercury isotope composition during a single precipitation event at Lhasa City, Tibetan Plateau. *China. Proced Earth Plan Sc* 13, 282–286.
- Yuan, W., Wang, X., Lin, C.J., Zhang, G., Wu, F., Liu, N., Jia, L., Zhang, H., Lu, H., Dong, J., 2024. Fate and Transport of Mercury through Waterflows in a Tropical Rainforest. *Environ. Sci. Technol.* 58 (11), 4968–4978.
- Zhang, Y.Y., Chen, J.B., Zheng, W., Sun, R.Y., Yuan, S.L., Cai, H.M., Yang, D.A., Yuan, W., Meng, M., Wang, Z.W., Liu, Y.L., Liu, J.F., 2020a. Mercury isotope compositions in large anthropogenically impacted Pearl River, South China. *Ecotoxicol. Environ. Saf.* 191, 110229.
- Zhang, Z.C., Chen, X., Cheng, Q.B., Soulsby, C., 2019. Storage dynamics, hydrological connectivity and flux ages in a karst catchment: conceptual modelling using stable isotopes. *Hydrol. Earth. Syst. Sci.* 23 (1), 51–71.
- Zhang, Z.C., Chen, X., Cheng, Q.B., Soulsby, C., 2020b. Characterizing the variability of transit time distributions and young water fractions in karst catchments using flux tracking. *Hydrol. Processes.* 34 (15), 3156–3174.
- Zhang, Z.C., Chen, X., Ghadouani, A., Shi, P., 2011. Modelling hydrological processes influenced by soil, rock and vegetation in a small karst basin of southwest China. *Hydrol. Processes.* 25 (15), 2456–2470.
- Zhao, L., Guo, Y.N., Meng, B., Yao, H., Feng, X.B., 2017. Effects of damming on the distribution and methylation of mercury in Wujiang River, Southwest China. *Chemosphere* 185, 780–788.
- Zhao, M., Liu, Z.H., Li, H.C., Zeng, C., Yang, R., Chen, B., Yan, H., 2015. Response of dissolved inorganic carbon (DIC) and  $\delta^{13}\text{C}$  to changes in climate and land cover in SW China karst catchments. *Geochim. Cosmochim. Acta* 165, 123–136.
- Zhao, M., Zeng, C., Liu, Z., Wang, S., 2010. Effect of different land use/land cover on karst hydrogeochemistry: A paired catchment study of Chenqi and Dengzhanhe, Puding, Guizhou, SW China. *J. Hydrol.* 388 (1-2), 121–130.
- Zheng, W., Hintelmann, H., 2009. Mercury isotope fractionation during photoreduction in natural water is controlled by its Hg/DOC ratio. *Geochim. Cosmochim. Acta* 73 (22), 6704–6715.
- Zheng, W., Hintelmann, H., 2010a. Isotope Fractionation of Mercury during Its Photochemical Reduction by Low-Molecular-Weight Organic Compounds. *J. Phys. Chem. A* 114 (12), 4246–4253.
- Zheng, W., Hintelmann, H., 2010b. Nuclear field shift effect in isotope fractionation of mercury during abiotic reduction in the absence of light. *The Journal of Physical Chemistry A* 114 (12), 4238–4245.
- Zheng, W., Liang, L., Gu, B., 2012. Mercury reduction and oxidation by reduced natural organic matter in anoxic environments. *Environ. Sci. Technol.* 46 (1), 292–299.